Hindawi
Journal of Mathematics
Volume 2022, Article ID 3950242, 21 pages
https://doi.org/10.1155/2022/3950242

Research Article

Simulation of Thermal Decomposition of Calcium Oxide in a Backward Step Tubular Reactor Containing a Cooling Jacket to Enhance the Heat Transfer and the Rotation Rate

Nawal A. Alshehri,[1] Abid A. Memon,[2] M. Asif Memon,[2,3] Bilawal A. Bhayo,[4] Kaleemullah Bhatti,[1] Hala A. Hejazi,[5] Kavikumar Jacob,[3] and Jamel Seidu[6]

[1]*Department of Mathematics and Statistics, College of Science, Taif University, P.O. Box 11099, Taif 21944, Saudi Arabia*
[2]*Department of Mathematics and Social Sciences, Sukkur IBA University, Sukkur, 65200 Sindh, Pakistan*
[3]*Department of Mathematics and Statistics, Faculty of Applied Sciences and Technology, Universiti Tun Hussein Onn Malaysia, Batu Pahat, 86400 Johar, Malaysia*
[4]*Department of Mechanical Engineering, Universiti Teknologi PETRONAS, Bandar Seri Islandar, 32610 Perak, Malaysia*
[5]*Mathematical Sciences Department, College of Applied Sciences, Umm Al-Qura University, Makkah, Saudi Arabia*
[6]*School of Railways and Infrastructure Development, University of Mines and Technology (UMaT) Essikado, Sekondi-Takoradi, Ghana*

Correspondence should be addressed to Jamel Seidu; jseidu@umat.edu.gh

Received 12 May 2022; Revised 30 June 2022; Accepted 30 September 2022; Published 19 October 2022

Academic Editor: A. M. Nagy

The chemical reactions widely operate in industries to enhance the heat transfer rate among the chosen domain. In the current article, we are going to observe an exothermic reaction of calcium oxide and water in a backward step tubular reactor with a cooled surrounded surface. The tubular reactor will be considered axisymmetric with an aspect ratio of 0.5, 0.6, and 0.7 from half radius to the length of the reactor. The governing partial differential equations of mass, momentum, and energy and diffusion equations are solved using the commercial package of finite element method of COMSOL Multiphysics 5.6. A parametric study is done by using the Reynolds number in the range and activation energy E in a range from 71,000 J/mol to 75,000 J/mol. The initial concentration of calcium oxide is tested from 1% to 3%. The computational results will be displayed for the upstream and downstream of the channel. It was concluded that the temperature difference is increasing linearly against the concentration of calcium hydroxide upstream and nonfunctional downstream. The average Sherwood and Nusselt numbers give a positive response with increasing the aspect ratio as well as the Reynolds number. The rotation rate at the middle of the downstream was also concluded using the Reynolds number and aspect ratio.

1. Introduction and Literature Review

For many decades, the chemistry of calcium oxide is extensively researched due to the production of renewable energies [1–4]. Calcium oxide is counted as one of the resources which are producing electricity and thermal light without any effect on the nature or the atmosphere. To acquire the energy stored, there are many procedures applied, but due to having the lowest cost, the chemical reactions are largely practiced. It is the quality of an exothermic reaction that yields the thermal density in a large quantity. Because of this reason, they are often considered in thermal storage procedures. The exothermic reaction of calcium oxide with water is widely studied due to its quick and easy availability in nature and low-cost efficiency in restoring the thermal energy storage [5–8]. Also, both reactants in this chemical reaction are nontoxic [9]. Due to the capability of the compound in storing energy, several applications can be found in mechanical industries to make the heat pumps [10–12], exclusion of carbon and energy storage [13–15],

getting hydrogen by sorption enhancement method [16, 17]. Several studies have been done with the transport of water with calcium oxide to achieve the knowledge of enthalpy of reaction and thermal equilibrium [18, 19]. A first-order chemical reaction was observed [20] of CaO and water by the pressure in the reactor between 50 and 500 kPa, and the size of particles in the mixture was considered 345.50 μm. The process of dehydration [21] via the use of calcium oxide was taken in an apparatus that can produce pressure in the range of 0.67 to 3.8 MPa. Keeping the temperature of 1023 K, it was found that the activation energy for the reaction was determined to be 8.8 kJ/mol. A chemical reaction of calcium oxide and steam [22] was numerically studied under the condition that the steam was kept at a high temperature of about 80 to 450°C, and then, a parametric study was done about changing the concentration from 1.5% to 22%. A bed reactor was observed by mixing the two compounds CaO and steam along with the nitrogen [23]. This study was done to express the heat and mass distribution along the length of the reactor.

The purpose of this article is to study the decomposition of calcium oxide in water in a backward tubular reactor containing a cooling jacket around the surface. The cooling jacket is created by imposing an inward heat flux condition around the surface. Different configurations of backward step tubular reactors will be observed by changing the aspect ratio between the half radius and length of the tubular reactor. About 225 simulations will be tested with the parametric study of Reynolds number, aspect ratio, activation energy, and percentage concentrations of the mixture at the inlet of the tubular reactor. First, we determine the grid interdependency of the simulation by doing a mesh independent study; later on, we would display the results for temperature difference, enthalpy, and Sherwood vs. local Nusselt number at the upstream and downstream of the channel. Finally, the computational results for the rotation rate will be displayed in the middle of the downstream of the channel.

2. Methodology

2.1. The Physical Construction of Tubular Reactor and Parameter Selection. An inverted backward step tubular reactor is investigated here for an exothermic reaction in which an irreversible reaction of water and calcium oxide is taken place. The simulation obtained in the channel is considered axisymmetric. Let "a" present the aspect ratio between the half-width and height of the downstream channel; then, the values of a will be assigned 0.5, 0.6, and 0.7 for the current simulation. The length of the channel in the axial direction is $L = 1$ m and in the radial direction is 0.2 m; see Figure 1. The left and right surfaces of this tubular reactor will perform as cooling jackets due to the reason that a constant inward heat flux of lower temperature $T_c = 273$ K will have pertained to it.

2.1.1. Chemical Reaction.

$$\mathrm{CaO} + \mathrm{H_2O} \longrightarrow \mathrm{Ca(OH)_2} \tag{1}$$

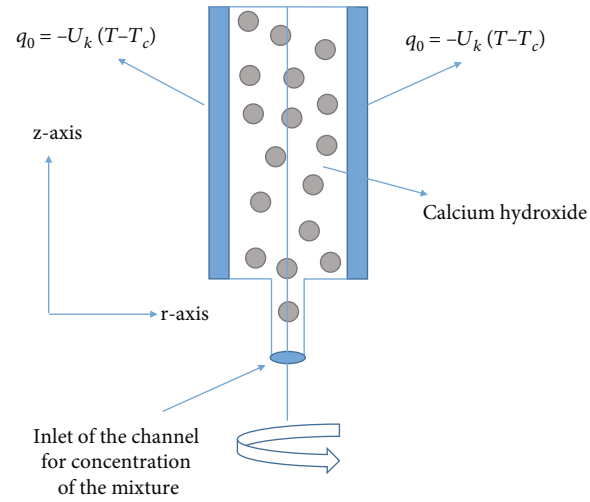

Figure 1: The geometry of the backward step channel and the boundary condition.

In the mixture, it is assumed that the water is present in excess. Therefore, the total rate of reaction depends upon the concentration of the calcium oxide which is now given by

$$R_n = k_f C_{\mathrm{CaO}}. \tag{2}$$

Here, k_f is the forward rate constant and measured by

$$k_f = Ae^{-E/RT}. \tag{3}$$

A hot temperature of $T_{\mathrm{in}} = 312$ K at the inlet of this tubular reactor is inflicted. The initial concentration of calcium oxide will be poured from the inlet with 1 to 3 percent in the water, which is considered the base fluid in the mixture. The reaction rate (2) where the forward rate constant is given by the Arrhenius equation (3). In the Arrhenius equation, we consider the frequency factor of $16.96E^{-12}$ 1/h which is taken to be constant throughout the different cases of problems, and for parametric study, we would consider the activation energy in the range from 71,000 to 75,000 J/mol K. Since the reaction is exothermic so it requires a negative heat of reaction of $\Delta H = -64{,}000$ J/mol. A parametric study will be evaluated for the Reynolds number in the range from 100 to 500 which will induce a total volume flow rate of 1.2×10^{-5} to 6.3×10^{-5}. The concentration amount of the calcium oxide as the initial concentration of the mixture is tested from 1% to 3%. To connect the volume flow rate and the Reynolds number, we are using the following two equations:

$$u_i = \frac{v_f}{\pi R_a^2}, \tag{4}$$

$$\mathrm{Re} = \frac{\rho_{\mathrm{water}} u_i L_c}{\mu_{\mathrm{water}}}. \tag{5}$$

Eliminating u_i equation (4) and putting in (5), we will

Table 1: Table of parametric selection.

Parameters	Value	Description
E	71,000 J/mol-75,000 J/mol	Activation energy
A	$16.96E^{12}$ [1/h]	Frequency factor
U_k	1300 W/m^2/K	Overall heat-transfer coefficient
κ	0.559 W/m/K	Thermal conductivity mixture
T_{in}	312 K	Inlet temperature
T_c	273 K	The inlet temperature of the coolant
ΔH	-64,300 J/mol	Heat of reaction
v_f	$1.2 \times E^{-5}$ m^3/s-$6.3 \times E^{-5}$ m^3/s	Total flow rate
$I.C$	1%-3%	Percentage concentration of calcium oxide as an initial concentration
c_{water}	43210 mol/m^3	Water concentration, inlet
R_a	0.2 m	Reactor radius
L	1 m	Reactor length
m_{CaO}	56.0774 g/mol	Molar weight, calcium oxide
m_{water}	18 g/mol	Molar weight, water
$m_{\text{Ca(OH)}_2}$	74.093 g/mol	Molar weight, calcium
ρ_{CaO}	3.34 g/cm^3	Density, calcium oxide
ρ_{water}	1000 kg/m^3	Density, water
$\rho_{\text{Ca(OH)}_2}$	2.24 g/cm^3	Density, calcium hydroxide
μ_{ref}	1e-3 Pas	Reference dynamic viscosity, water
T_{ref}	293 K	Reference temperature viscosity
c_p	75.36 J/mol/K	Molar heat capacity, water
Re	100-500	Reynolds number

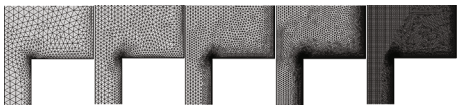

Figure 2: Different configurations of the mesh setting from normal to extremely fine mesh.

have

$$\text{Re} = \frac{\rho_{\text{water}} v_f L_c}{\mu_{\text{water}} \pi R_a^2}. \tag{6}$$

Further detail for the parametric selection is given in Table 1.

2.2. Boundary Conditions and Constitutive Partial Differential Equations. It is the circumstance of large care to test an exothermic reaction in the tubular reactor because of a reasonable explosion. Therefore, a surface is a desire that can deliver the cooling environment inside the backward step reactor called a cooling suit or jacket. For this purpose, inward heat flux is operated inside the tube with a constant cooling temperature. A very dense mesh was applied to obtain the numerical results with the use of finite element-based algorithms through the software COMSOL Multiphysics 5.6. We achieved simulation for this exothermic reaction of calcium oxide and water to discretize the governing partial differential equations of mass, momentum, and energy balance equations for an axisymmetric channel. Moreover,

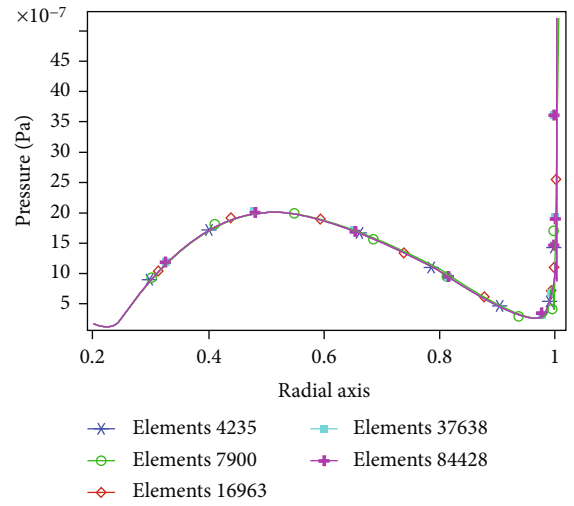

Figure 3: The computational results for the pressure downstream of the channel at the different configurations of meshes.

the chemical engineering interface was also utilized to analyze this first-order reaction.

Initially, it was assumed that the mass diffusivity of each species is considered the same throughout the domain selected for diffusion. We also indicate that the current exothermic reaction will be handled by 5 partial differential equations and one ordinary differential equation. Out of six ordinary or partial differential equations, two of them will handle mass diffusion, two are used to handle momentum, and one is used for mass balance. Lastly, the most important equation that will balance the hot environment is the backward step channel; the ordinary differential equation will be solved for the surface of the channel. All these governing equations are given in detail:

$$\frac{1}{r}\frac{\partial(rv_r)}{\partial r}+\frac{\partial(v_z)}{\partial z}=0,$$

$$\frac{1}{r}\frac{\partial}{\partial r}(rv_rv_r)+\frac{\partial}{\partial z}(rv_rv_z)=\frac{\mu}{\rho}\left\{\frac{2}{r}\frac{\partial}{\partial r}\left(r\frac{\partial v_r}{\partial r}\right)+\frac{\partial}{\partial z}\left(r\frac{\partial v_r}{\partial z}\right)-2\frac{v_r}{r^2}+\frac{\partial}{\partial z}\left(\frac{\partial v_z}{\partial r}\right)\right\}-\frac{1}{\rho_{\text{water}}}\frac{\partial p}{\partial r},$$

$$\frac{1}{r}\frac{\partial}{\partial r}(rv_rv_z)+\frac{\partial}{\partial z}(rv_zv_z)=\frac{\mu}{\rho}\left\{\frac{1}{r}\frac{\partial}{\partial r}\left(r\frac{\partial v_z}{\partial r}\right)+2\frac{\partial}{\partial z}\left(\frac{\partial v_z}{\partial z}\right)+\frac{1}{r}\frac{\partial}{\partial r}\left(r\frac{\partial v_r}{\partial z}\right)\right\}-\frac{1}{\rho_{\text{water}}}\frac{\partial p}{\partial z},$$

$$v_r\frac{\partial T}{\partial r}+v_z\frac{\partial T}{\partial z}=\frac{k}{\rho c_p}\left\{\frac{\partial}{\partial z}\left(\frac{\partial T}{\partial z}\right)+\frac{1}{r}\frac{\partial}{\partial r}\left(r\frac{\partial T}{\partial r}\right)\right\}+(-\Delta H)\frac{R_n}{\rho_{\text{water}}c_p},$$

$$v_r\frac{\partial C}{\partial r}+v_z\frac{\partial C}{\partial z}=\frac{k}{\rho c_p}\left\{\frac{\partial}{\partial z}\left(\frac{\partial C}{\partial z}\right)+\frac{1}{r}\frac{\partial}{\partial r}\left(r\frac{\partial C}{\partial r}\right)\right\}-\frac{1}{\rho_{\text{water}}c_p}R_n,$$

$$\frac{\partial T}{\partial r}=\frac{U_k}{k}(T-T_c).\ - \tag{7}$$

2.2.1. Boundary Conditions. At inlet of the reactor $z=0$,

$$C(r,0)=\text{initial concentration}=c_0,\ T(r,0)=T_{\text{in}},\ v_z=\text{inlet velocity}=u_i=f(\text{Re}). \tag{8}$$

At outlet of the reactor $z=L$,

$$\frac{\partial C}{\partial r}(r,L)=0,\ -\frac{\partial T}{\partial r}(r,L)=0,\ p=0. \tag{9}$$

Around the wall of the reactor $r=R_a$,

$$\frac{\partial C}{\partial r}=0,\ -\frac{\partial T}{\partial r}=\frac{U_k}{k}(T-T_0). \tag{10}$$

2.2.2. Computational Parameters.

$$\text{Viscosity}=\mu=10^{-3}\left[\left(\mu_{\text{ref}}10^3\right)^{-0.2661}+\frac{T-T_{\text{ref}}}{223}\right]^{-3.758}, \tag{11}$$

$$\text{Molar concentration}=M_{\text{CaO}}=\frac{\text{moles of solution}}{\text{total solution in liters}}, \tag{12}$$

$$\text{Thermal diffusivity of calcium oxide}=D_{\text{CaO}}=\frac{7.4\times10^{-8}T\chi\sqrt{M_{\text{H}_2\text{O}}}}{\eta\left(M_{\text{CaO}}/\rho_{\text{CaO}}\right)^{0.6}}. \tag{13}$$

Equation (13) is given by Wilke-Chang [24] and is known to be the correlation to determine the diffusion of a compound in a solvent. In this equation, χ is the solution index which is taken to be 1 for nonassociated solvent, and for water, it can be taken as 2.26. The further computational results will be presented for the following parameters:

$$\text{Local Nusselt number}=\text{Nu}_z=\frac{\text{convective heat transfer}}{\text{conductive heat transfer}}=\frac{U_kz}{k},$$

$$\text{Sherwood number}=\text{Sh}=\frac{\text{convective mass transfer rate}}{\text{diffusion rate}}=\frac{h}{D_{\text{CaO}}/L},$$

$$\text{Prandtl number}=\text{Pr}=\frac{\text{momentum diffusivity}}{\text{thermal diffusivity}}=\frac{\mu c_p}{k}. \tag{14}$$

It is commonly observed in the fluid flow phenomenon when the fluid is entered the downstream of the channel, a vortex was found which is recirculating along the corner of the downstream. In the current problem, we have tried to find the rotation rate downstream of the channel. So ω is the rotation rate of the fluid downstream of the channel. Then, by the definition of the rotation rate, we can write the equation as

$$\omega=\sqrt{\frac{1}{2}\left(\frac{\partial v_r}{\partial z}-\frac{\partial v_z}{\partial r}\right)^2+\frac{1}{2}\left(\frac{\partial v_z}{\partial r}-\frac{\partial v_r}{\partial z}\right)^2}. \tag{15}$$

2.3. Mesh Independent Study. To get better results in terms of accuracy, the mesh independent study is performed in this section. This can be regarded as a crucial step of the finite element method. It indicates the maximum number of elements in such a way the targeted variable is not improving further even with the increase in the number of

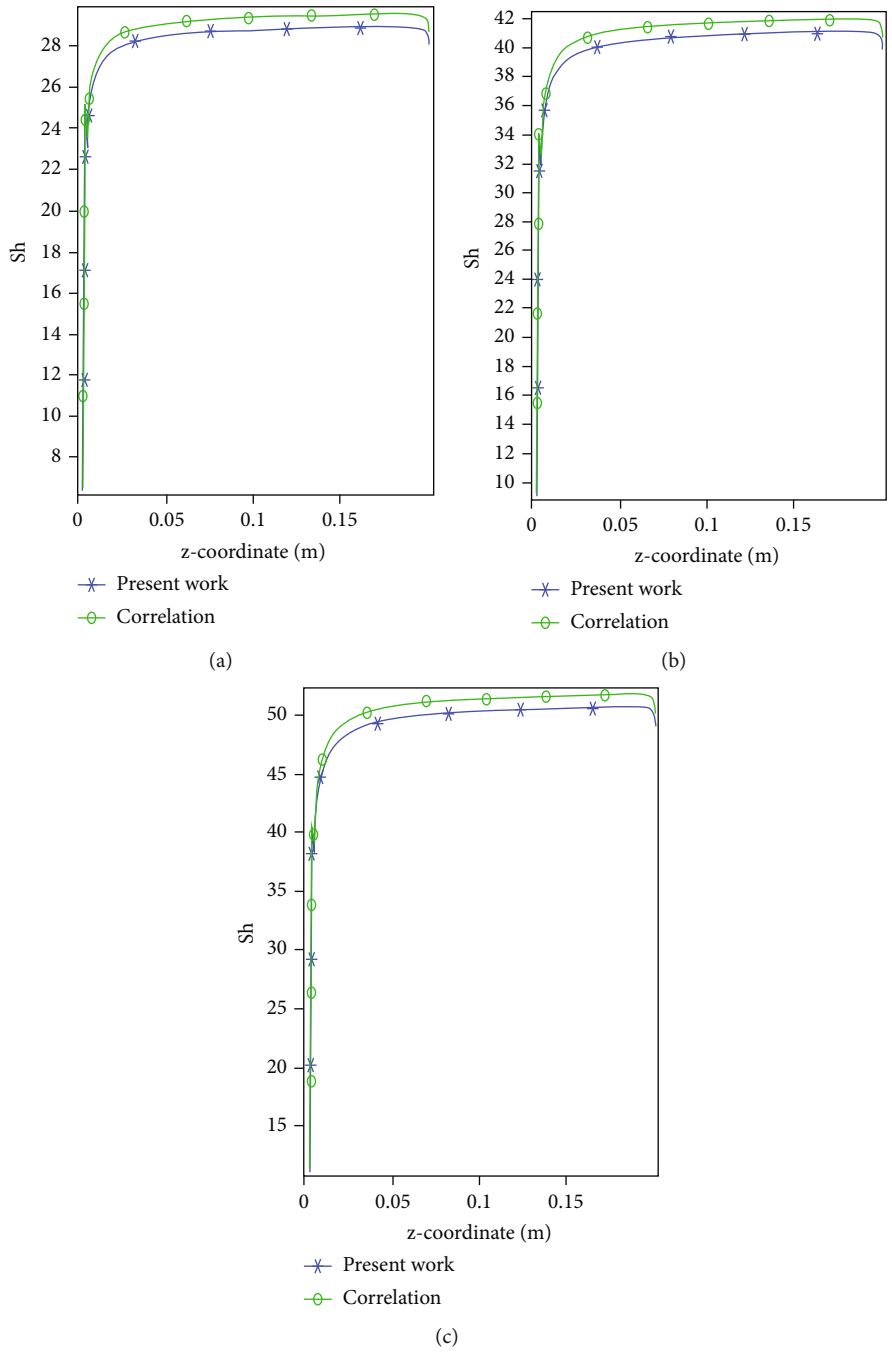

Figure 4: The comparison of the Sherwood number at the vicinity of inlet with the correlation available from the literature at $E = 71{,}000$ J/mol: (a) Re = 100, (b) Re = 200, and (c) Re = 300.

elements in the meshing process. It is easy to say the solution will become mesh-independent. The domain of interest will be discretized by the use of distinctive triangular elements. Figure 2 demonstrates the zoom-in picture of the meshing process and the different configuration of triangular elements that varies from normal to extremely fine. The minimum number of elements is chosen about 4235 for the meshing process to get the targeted variable pressure downstream of the channel. Figure 3 indicates the computational effects of the pressure. Although, the pressure downstream is increasing up to the middle and then decreasing, the pressure at the outlet is increasing at a high rate as well as high magnitude. About 84,428 irregular triangular elements are used to boost the numerical results for the pressure. Figure 3 demonstrates the mesh independence of the numerical technique. As it reveals that the numerical values of the pressure at the downstream achieve a mesh independent when 84,428 elements are employed, it can also be

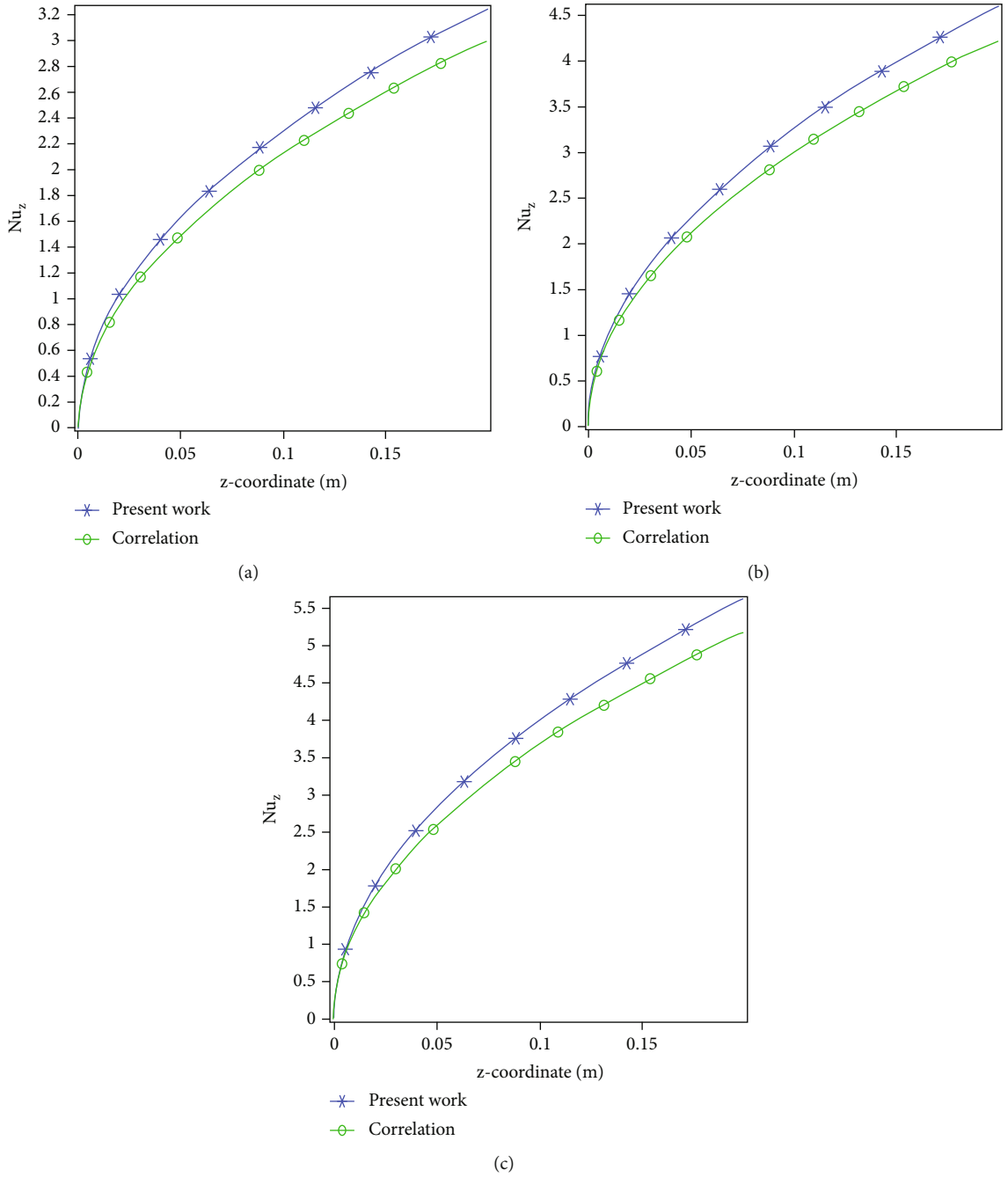

Figure 5: The comparison of the Nusselt number at the vicinity of inlet with the correlation available from the literature at $E = 71{,}000$ J/mol: (a) Re = 100, (b) Re = 200, and (c) Re = 300.

detected from outcomes that the pressure at the outlet for this mixture is getting an unexpected hike in values.

$$\mathrm{Sh}_D = 0.3 + \frac{0.62\,\mathrm{Re}^{1/2}\mathrm{Sc}^{1/3}}{\left[1 + (0.4/\mathrm{Sc})^{2/3}\right]^{1/4}}\left[1 + \left(\frac{\mathrm{Re}}{282000}\right)^{5/8}\right]^{4/5}, \tag{16}$$

$$\mathrm{Nu}_z = 0.032\,\mathrm{Re}_z^{1/2}\mathrm{Pr}^{1/3}. \tag{17}$$

To validate the numerical results obtained by using the software COMSOL Multiphysics, we are comparing the numerical results for Sherwood number and the Nusselt number at very near to the inlet of channel with the results obtained by the correlations (16) and (17) [25, 26]; see Figures 4 and 5. It can be seen that the numerical results are in a good fit with that of results obtained by the correlations. Equation (16) is based on the analogy that the Sherwood number can be used in the same way to predict the performance of mass transfer as the Nusselt number does in the case of heat transfer. Also, it suggests the analogy can be followed when the Prandtl number is replaced by

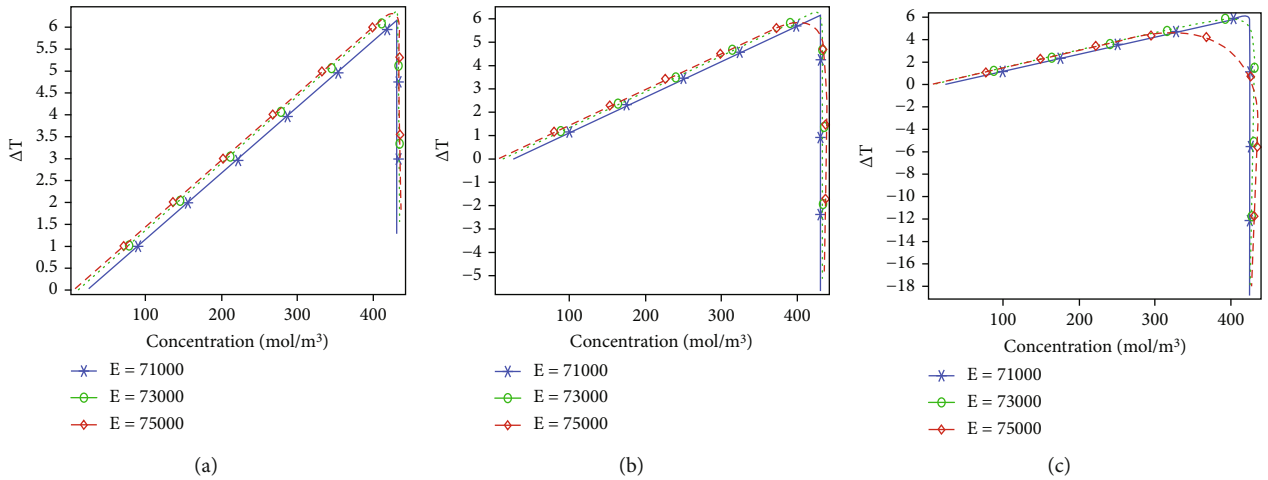

Figure 6: Change in the temperature at upstream along the backward step channel against the concentration of calcium hydroxide at (a) Re = 100, $I.C = 1\%$, $a = 0.5$; (b) Re = 100, $I.C = 1\%$, $a = 0.6$; and (c) Re = 100, $I.C = 1\%$, $a = 0.7$.

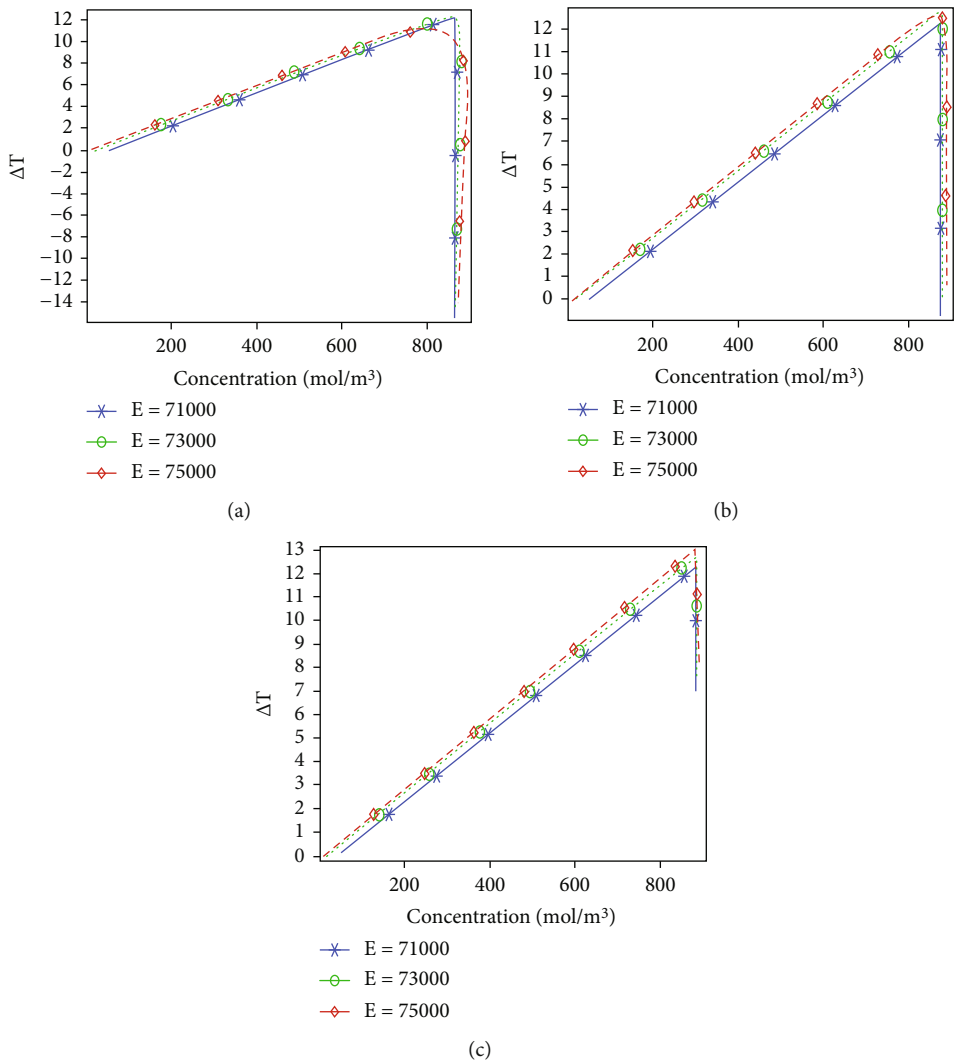

Figure 7: Change in the temperature at upstream along the backstep channel against the concentration of calcium hydroxide at (a) Re = 100, $I.C = 2\%$, $a = 0.5$; (b) Re = 100, $I.C = 2\%$, $a = 0.6$; and (c) Re = 100, $I.C = 2\%$, $a = 0.7$.

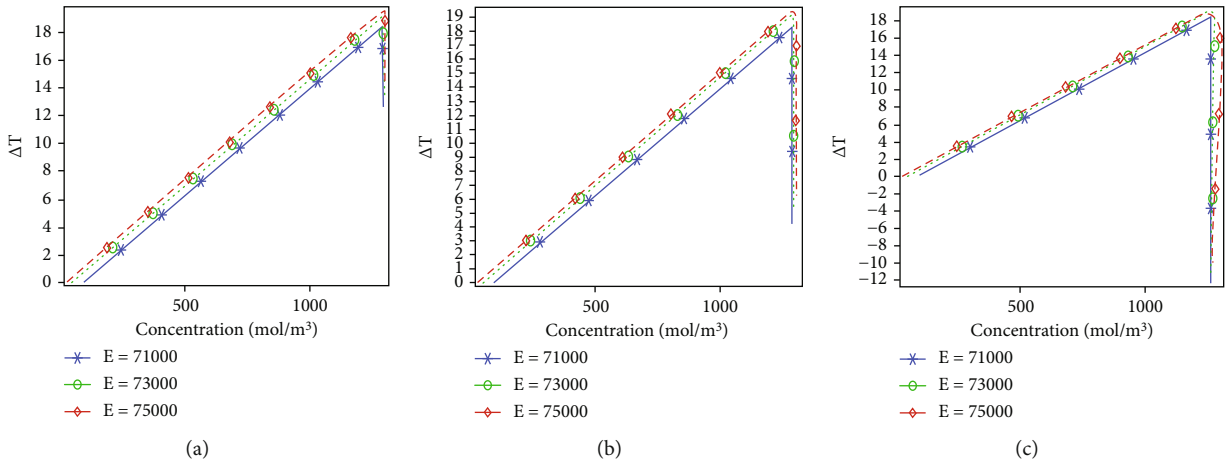

Figure 8: Change in the temperature at upstream along the backstep channel against the concentration of calcium hydroxide at (a) Re = 100, $I.C = 3\%$, $a = 0.5$; (b) Re = 100, $I.C = 3\%$, $a = 0.6$; and (c) Re = 100, $I.C = 3\%$, $a = 0.7$.

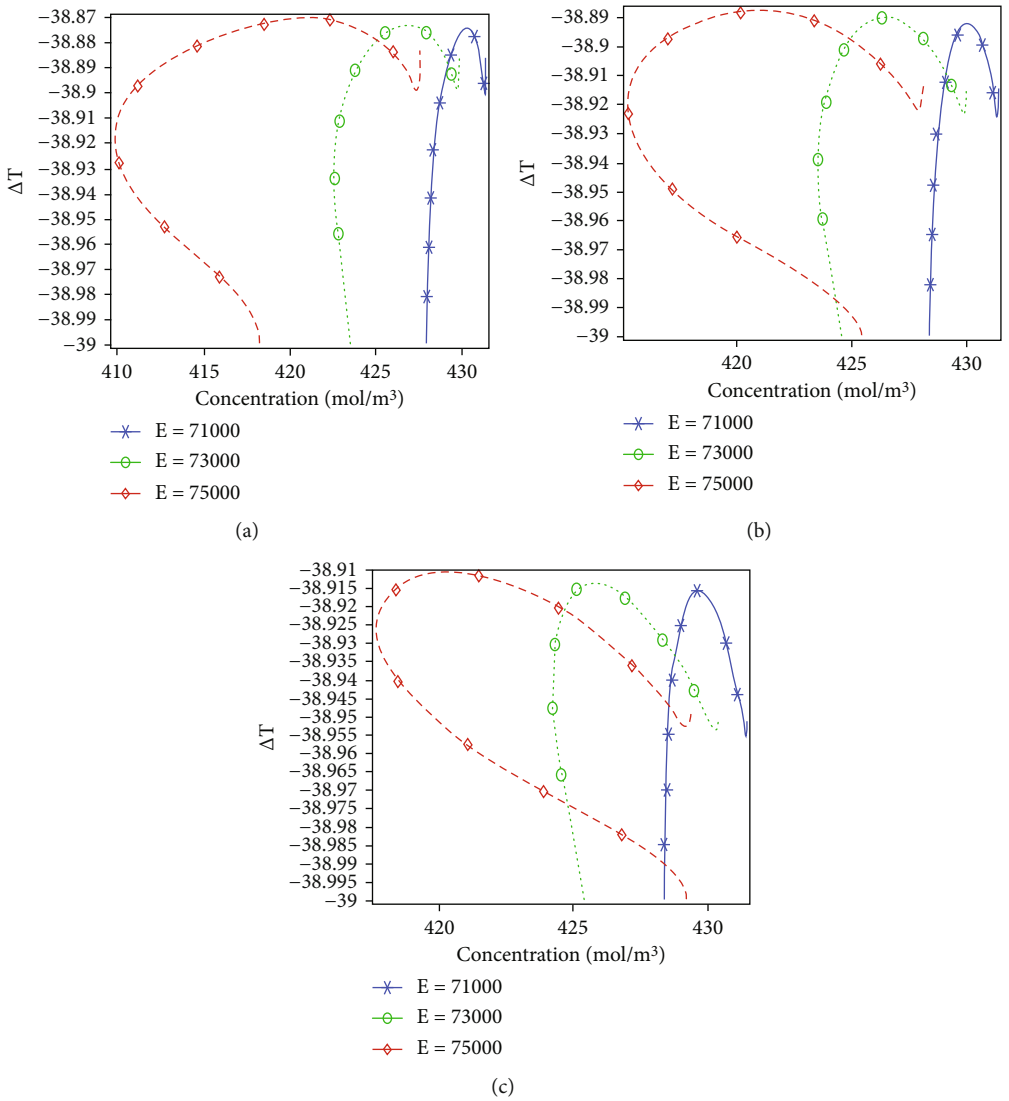

Figure 9: Change in the temperature at downstream along the backward step channel against the concentration of calcium hydroxide at (a) Re = 100, $I.C = 1\%$, $a = 0.5$; (b) Re = 100, $I.C = 1\%$, $a = 0.6$; and (c) Re = 100, $I.C = 1\%$, $a = 0.7$.

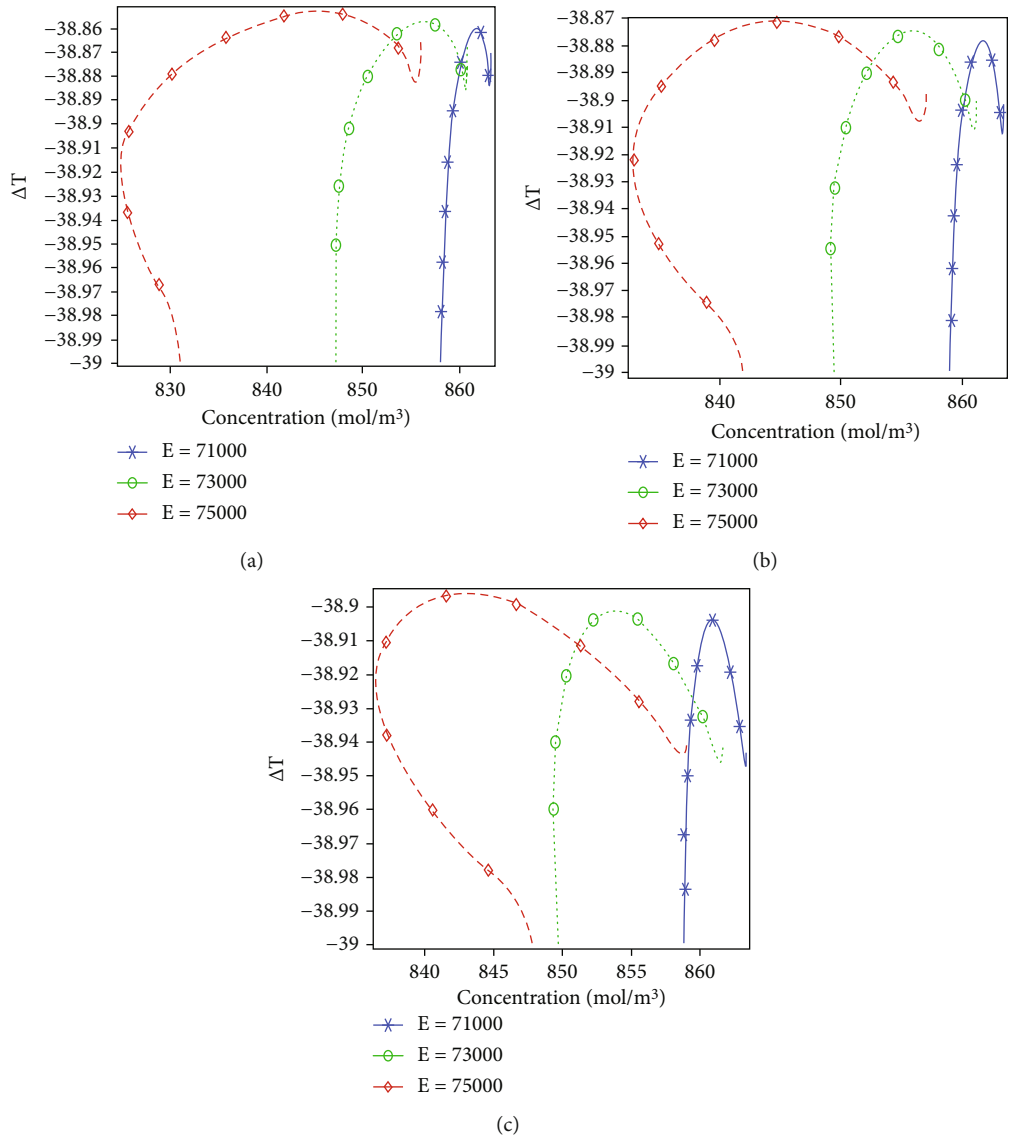

Figure 10: Change in the temperature at downstream along the backward step channel against the concentration of calcium hydroxide at (a) Re = 100, $I.C = 2\%$, $a = 0.5$; (b) Re = 100, $I.C = 2\%$, $a = 0.6$; and (c) Re = 100, $I.C = 2\%$, $a = 0.7$.

the Schmidt number in the correlation that connects the Nusselt number and the Prandtl number.

3. Result Discussion

3.1. Temperature Difference at the Upstream and Downstream of Backward Step Channel. Here, we examine an inverted backward step channel for an exothermic reaction of water and calcium oxide using the dimensional and nondimensional parameters. We made maximum efforts using these parameters to get a maximum heat transfer rate in the selected domain. The mixture is allowed to in facing the temperature $T_{in} = 273$ K, whereas around the surface of this tubular reactor a cooling suit is maintaining a cooling environment. In this exothermic reaction, calcium oxide reacts with water to produce calcium hydroxide. In this section, we are going to measure how much the quantity of calcium hydroxide evolves to maintain the temperature difference $\Delta T = T - T_{in}$ inside the tube. For this purpose, we are producing the graphs (Figures 6–11) which measured the temperature difference of the upstream and downstream of the channel. In Figures 6(a)–6(c), the temperature difference is measured for a 1% concentration of calcium oxide with different aspect ratios a that produced a maximum concentration of calcium hydroxide between 400 and 450.

The temperature difference is increasing linearly and reaches the maximum level at the outlet of the channel, and after that, temperature difference is decreasing. With the increasing aspect ratio, it seems that the maximum temperature difference is achieved as a maximum output at the outlet, and the temperature difference is cooled down with a maximum range of -ve values. Also, it can be seen that with increasing activation energy, the temperature difference along the domain is a little bit increasing. In Figures 7(a)–7(c), the temperature difference is also measured with a concentration of 2% in calcium oxide with different aspect ratios

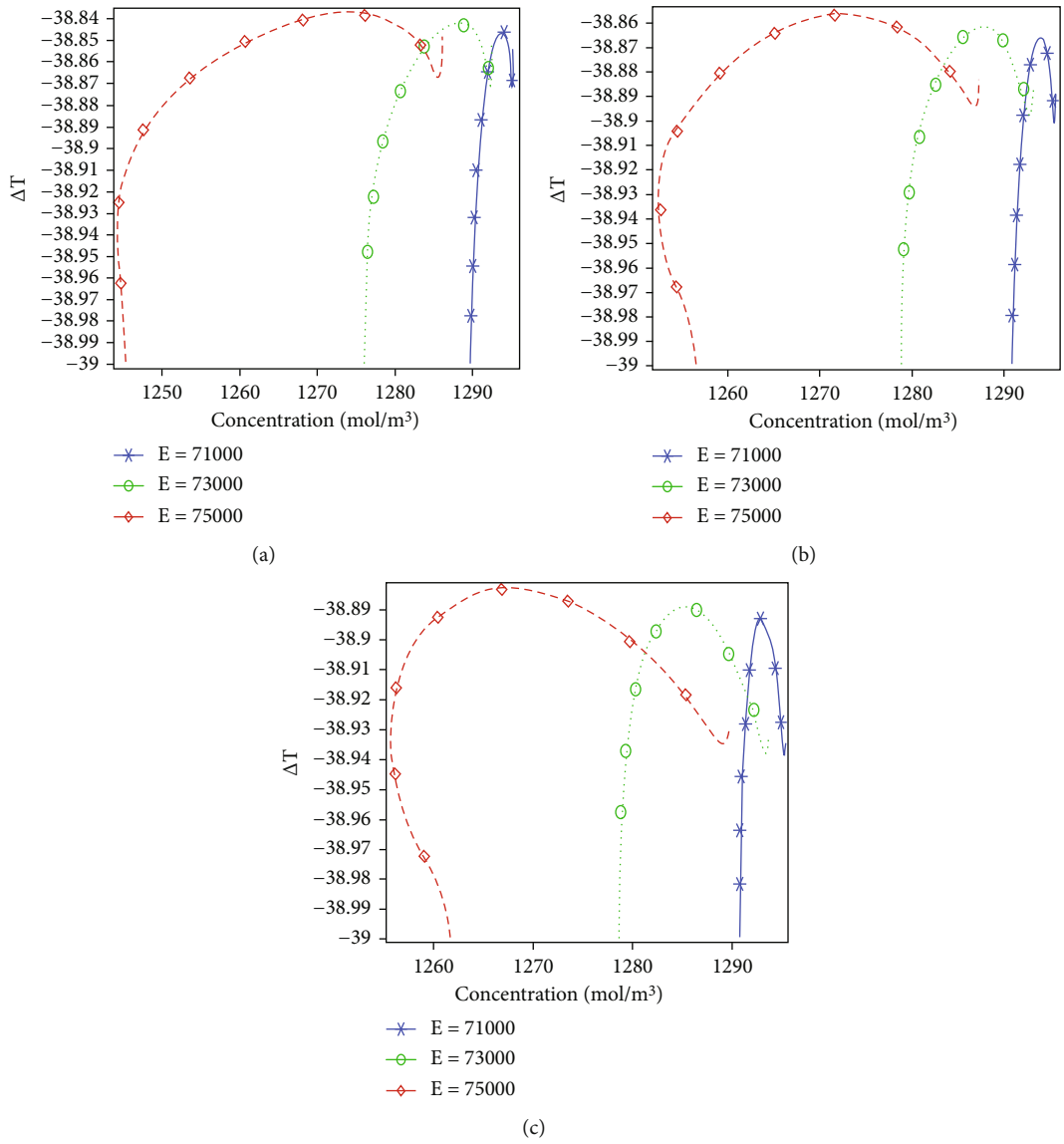

Figure 11: Change in the temperature at downstream along the backward step channel against the concentration of calcium hydroxide at (a) Re = 100, $I.C = 3\%$, $a = 0.5$; (b) Re = 100, $I.C = 3\%$, $a = 0.6$; and (c) Re = 100, $I.C = 3\%$, $a = 0.7$.

and activation energy. The concentration of calcium hydroxide is produced 850 mol/m^3 within all aspect ratios. Moreover, the maximum temperature at the outlet is increasing with increasing activation energy.

A negative temperature difference can be seen for only aspect ratio $a = 0.5$. These graphs are also indicating that with the change of 1% initial concentration of calcium oxide the maximum difference in the temperature from inlet to onwards becomes twice. The temperature difference at the outlet is also decreasing in the case as in case of the 1% initial concentration of calcium oxide. The temperature difference for the 3% initial concentration of calcium oxide is presented in Figures 8(a)–8(c). It can be noted that the maximum temperature at the outlet is increasing with the increase in activation and twice when compared to the 1% concentration. Also, we found a negative temperature difference at the outlet in the case of $a = 0.7$.

We also intended to evaluate the temperature difference downstream in the channel. It can be seen in Figures 9–11(c) that the concentration of calcium hydroxide downstream of the channel was found to be half of the concentration upstream of the channel; see Figures 9(a)–9(c). With all aspect ratios, the minimum temperature difference is the same as the downstream and which is found to be -39 K. The temperature difference downstream of the channel is getting improved due to an increase in the activation energy. Unlike the temperature difference upstream in the channel, we found that a cooling environment has been created downstream of the channel. The reason behind this is an inward heat flux condition applied on the lower boundary of the channel.

From Figures 9(a)–10(c), it can be noted that the temperature difference for the activation energy $E = 75{,}000$ J/mol is not a function concentration of the calcium

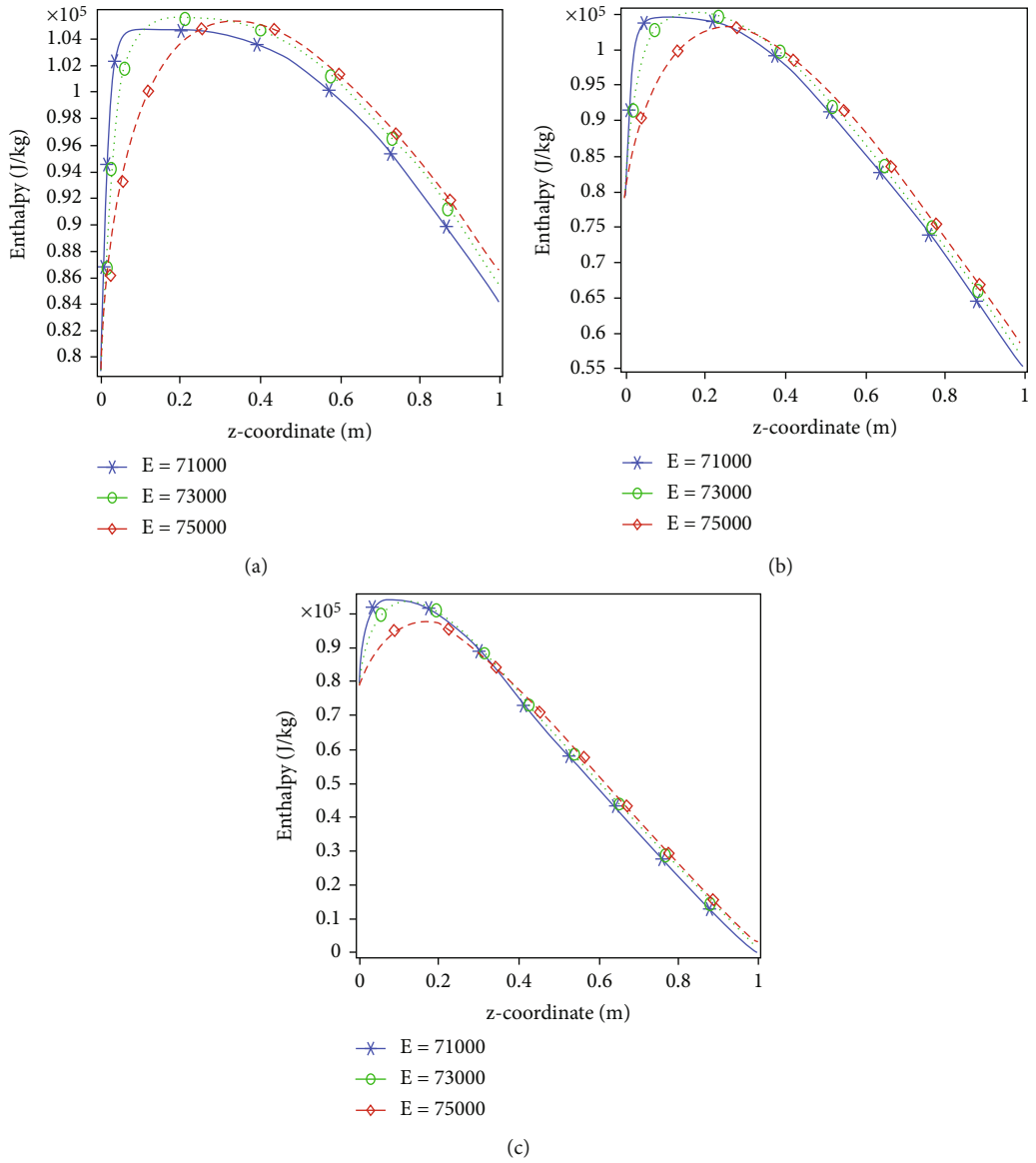

FIGURE 12: Measurement of enthalpy at upstream along the backward step channel against the axial direction at (a) Re = 100, $I.C = 1\%$, $a = 0.5$; (b) Re = 100, $I.C = 1\%$, $a = 0.6$; and (c) Re = 100, $I.C = 1\%$, $a = 0.7$.

hydroxide. But for the activation energy $E = 71{,}000$-$73{,}000$ J/mol, the temperature difference was found to be the function of the concentration of calcium hydroxide whenever the concentration of calcium hydroxide is evaluated for the cases of 1% and 2% as the initial concentration of calcium oxide, enough to have a cooling environment around the surface of this backward step tubular reactor, but the temperature difference downstream of the channel is increasing along the length and attempts the maximum magnitude along the middle of the length. That can be observed from all graphs in Figures 9–11(c). In comparison with the case when the temperature was evaluated upstream of the tubular reactor, the temperature difference was increasing linearly against the length of the temperature, but in the present case, the temperature difference shows a parabolic variation against the length of the reactor.

3.2. Enthalpy Production at the Upstream and Downstream of the Channel. The sensible enthalpy or simple enthalpy will be described in the section against the selected parameters at the upstream and downstream of the channel; see Figures 12–15(c). In Figure 12(a), it can be seen that rapid increments in the enthalpy were observed near the outlet of the channel. The pattern of distribution of enthalpy along the channel is parabolic; i.e., it is increasing first from the inlet and attempt a maximum value then decreases up to the outlet of the channel. For particular cases in Figures 12(a)–13(c), the value of enthalpy starts from 0.8×10^5. It is also indeed from these graphs that for a lower aspect ratio in the channel, the enthalpy increases rapidly and reaches the maximum value and then decreases and reaches zero value at the outlet depending upon the initial concentration. With the increase in initial concentration at

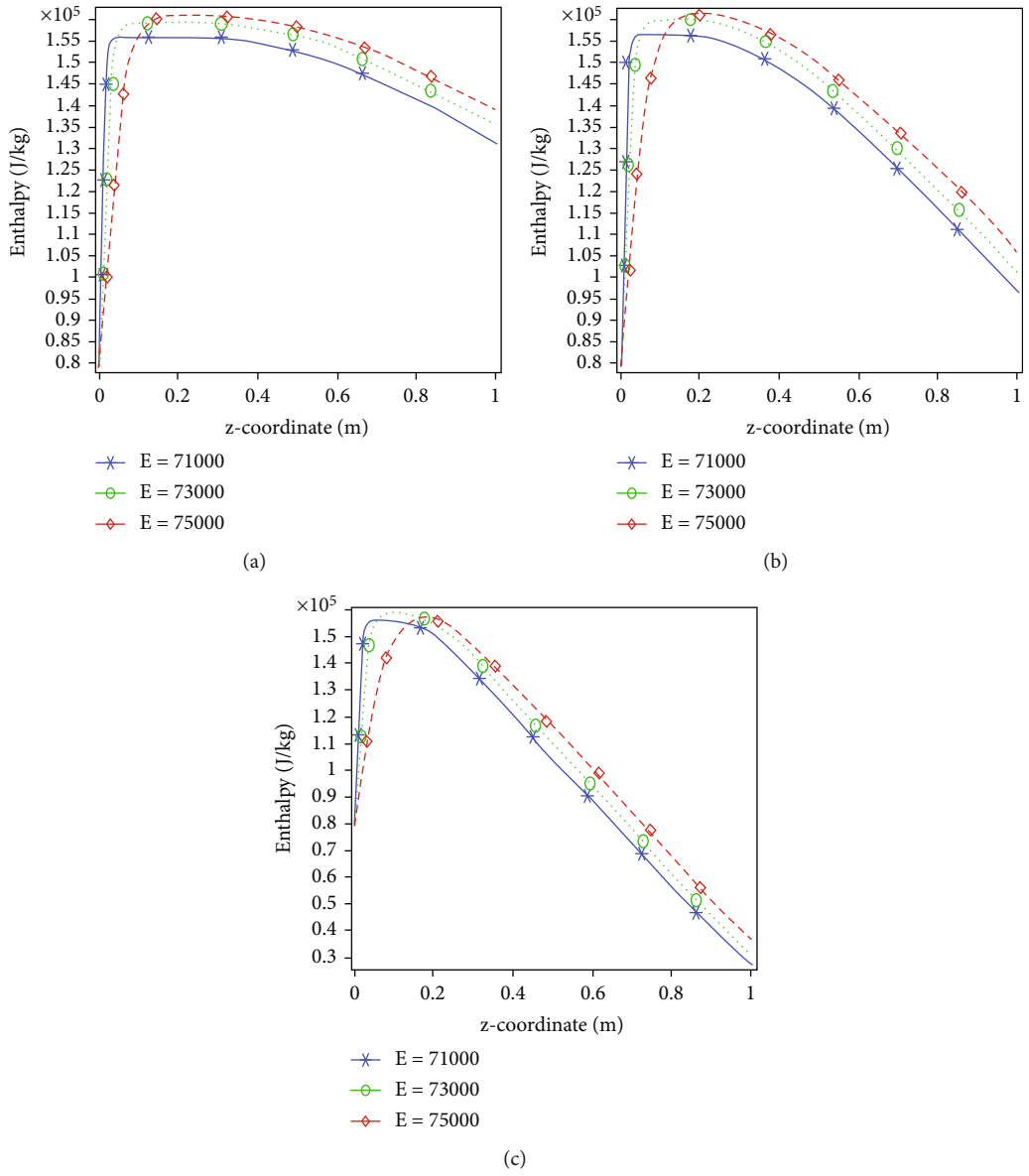

Figure 13: Measurement of enthalpy at upstream along the backward step channel against the axial direction at (a) Re = 100, $I.C = 3\%$, $a = 0.5$; (b) Re = 100, $I.C = 3\%$, $a = 0.6$; and (c) Re = 100, $I.C = 3\%$, $a = 0.7$.

the outlet of the channel, the maximum enthalpy before the start of the inlet is also increased.

The computational results for enthalpy are also produced downstream in the channel; see Figures 14(a)–15(c). It can be seen that the enthalpy produced downstream of the channel is negative. The starting value of the enthalpy in all the cases (Figures 14(a)–15(c)) is -83,350 J/mol to onwards. Enthalpy in the downstream of the channel is increasing the first attempt a maximum value and then decreases up to the outlet of the channel. Although it can be seen that the enthalpy before reaching the outlet of the channel is increasing again, the maximum enthalpy is increasing with the increase in activation energy provided initially; see Figures 12(a)–12(c). But the maximum enthalpy is also increased if we provided a more initial concentration of the calcium oxide; see Figures 15(a)–15(c). One point should be also added that to get maximum enthalpy at the downstream, keep initial concentration very high at the outlet and as well as the aspect ratio of the channel for fixed initial concentration.

3.3. Sherwood Number vs. Local Nusselt Number at Upstream and Downstream. In the section, we are going to investigate the pattern of reaction of Sherwood number and local Nusselt number at the upstream and downstream in the channel in Figures 16–19(c), respectively. It can be detected in Figures 16(a) and 17(a) at the activation energy of 71,000 J/mol and $a = 0.5$ that the Sherwood number is decreasing

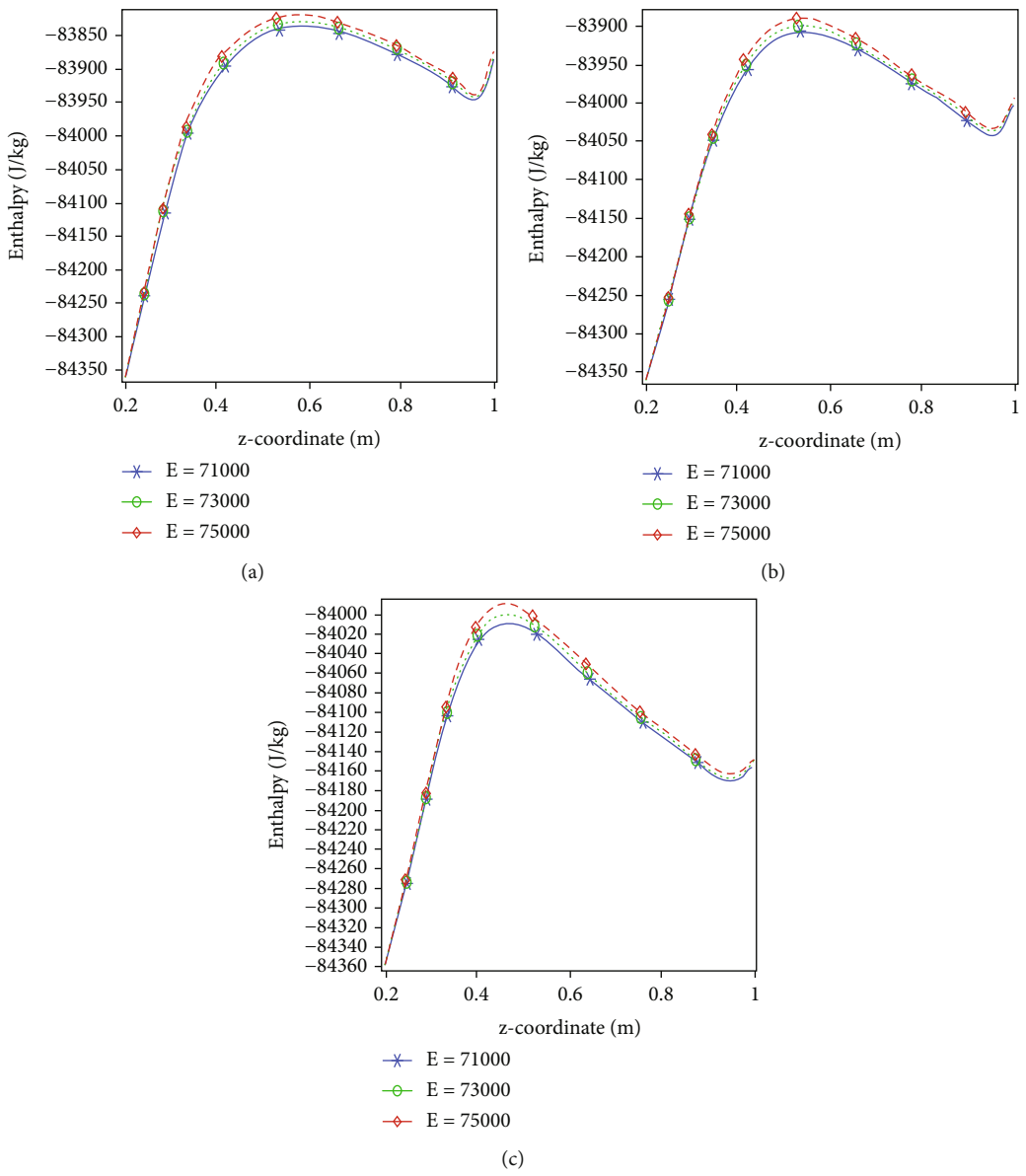

Figure 14: Measurement of enthalpy at downstream along the backstep channel against the axial direction at (a) Re = 100, $I.C = 1\%$, $a = 0.5$; (b) Re = 100, $I.C = 1\%$, $a = 0.6$; and (c) Re = 100, $I.C = 1\%$, $a = 0.7$.

with an increase in local Nusselt number up to the middle of the channel and then increasing up to the outlet of the channel. With a little boost in activation energy, the Sherwood number is also decreasing with increasing local Nusselt but with a lower rate, when compared with the case of lower activation energy. With the increasing aspect ratio, the Sherwood number is increasing at the outlet against the local Nusselt number. A rapid increment in the Sherwood number against the local Nusselt number can be detected upstream for all cases in Figures 16(a)–17(c). This rapid increment in Sherwood number is increasing with an increase in the aspect ratio of the channel.

The values of the Sherwood number downstream of the channel were found higher than the values the upstream. The structure or behavior of the Sherwood concerning the local Nusselt number is the same but with increasing activation energy initially, decreasing the values of the Sherwood number for all the cases in Figures 18(a)–18(c). The Sherwood number first decreases with an increase in the local Nusselt number up to the middle of the channel and then increases. In all cases, the Sherwood number downstream possesses a nonlinear relationship with the local Nusselt number. It can be said that on behalf of comparison for these two cases for Sherwood number at the upstream and downstream, the convection rate at the downstream is always greater than upstream. Figures 16(a) and 18(a) can be compared in this regard. An insignificant change was found in the relationship between Sherwood number and the local

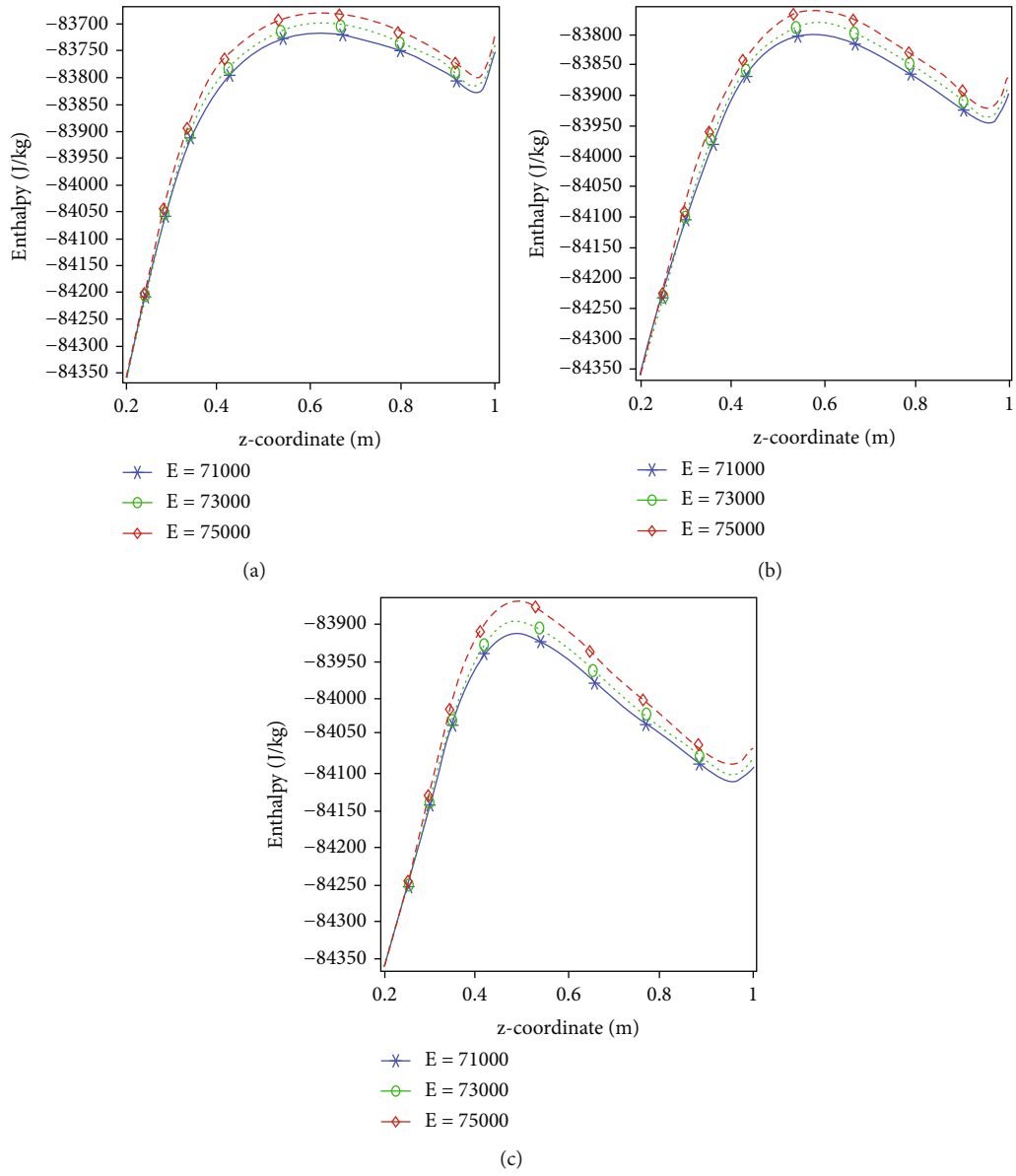

FIGURE 15: Measurement of enthalpy at downstream along the backstep channel against the axial direction at (a) Re = 100, $I.C = 3\%$, $a = 0.5$; (b) Re = 100, $I.C = 3\%$, $a = 0.6$; and (c) Re = 100, $I.C = 3\%$, $a = 0.7$.

Nusselt with the increase of the initial concentration of calcium oxide at the inlet. The impact can be seen either in upstream cases Figures 16–17(c) or in downstream cases Figures 18–19(c). Finally, we are displaying the table showing the average Sherwood number and average Nusselt number at the outlet for all the cases in Table 2.

From Table 2, it is clearer that the average Sherwood number and the average Nusselt number are increasing at the outlet with increasing the aspect ratio and the Reynolds number whereas decreasing with the increasing initial concentration and the activation energy.

3.4. Rotation Rate in the Middle of the Downstream of the Channel. The equation for rotation rate is already stated in Boundary Conditions and Constitutive Partial Differential Equations. Here, we are going to describe the pattern of the rotation rate with the impact of Reynolds number, aspect ratio, initial concentration, and the activation energy. In Figures 20(a) and 20(b), the rotation rate is calculated with a fixed aspect ratio $a = 0.5$ with different initial concentrations. It can be seen that the rotation rate in each case first approaches zero and starts increasing up to the outlet of the channel. Before approaching the outlet, a rapid increment can be seen for all cases. In each case, an increment in the Reynolds number increases the rotation rate gradually. The pattern of the rotation rate is zigzag not smooth as obvious from Figures 20(a) and 20(b). However, a small increment can be seen at the outlet of the channel when

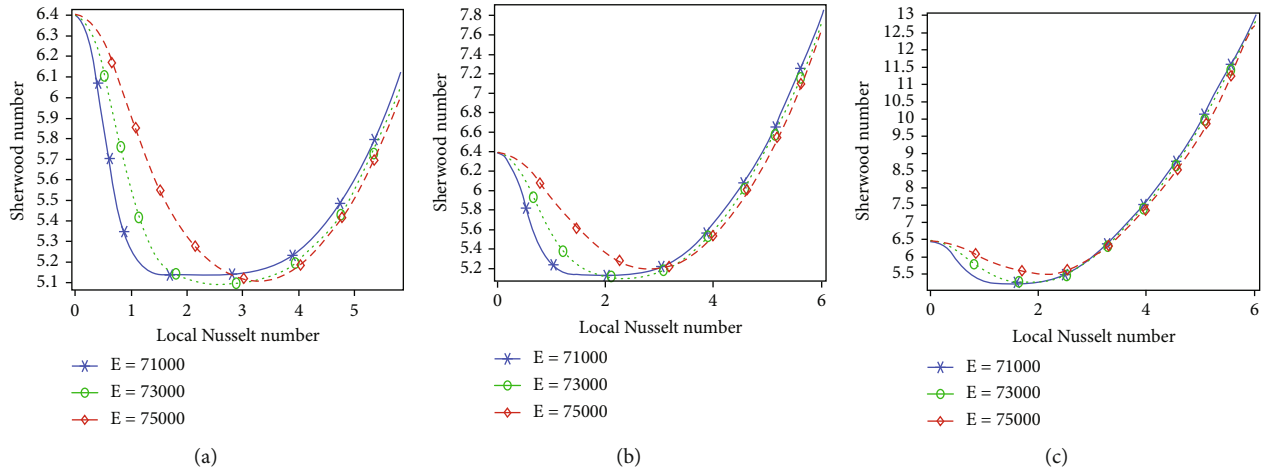

FIGURE 16: Sherwood number vs. the local Nusselt number at upstream along the backward step channel against the axial direction at (a) Re = 100, $I.C = 1\%$, $a = 0.5$; (b) Re = 100, $I.C = 1\%$, $a = 0.6$; and (c) Re = 100, $I.C = 1\%$, $a = 0.7$.

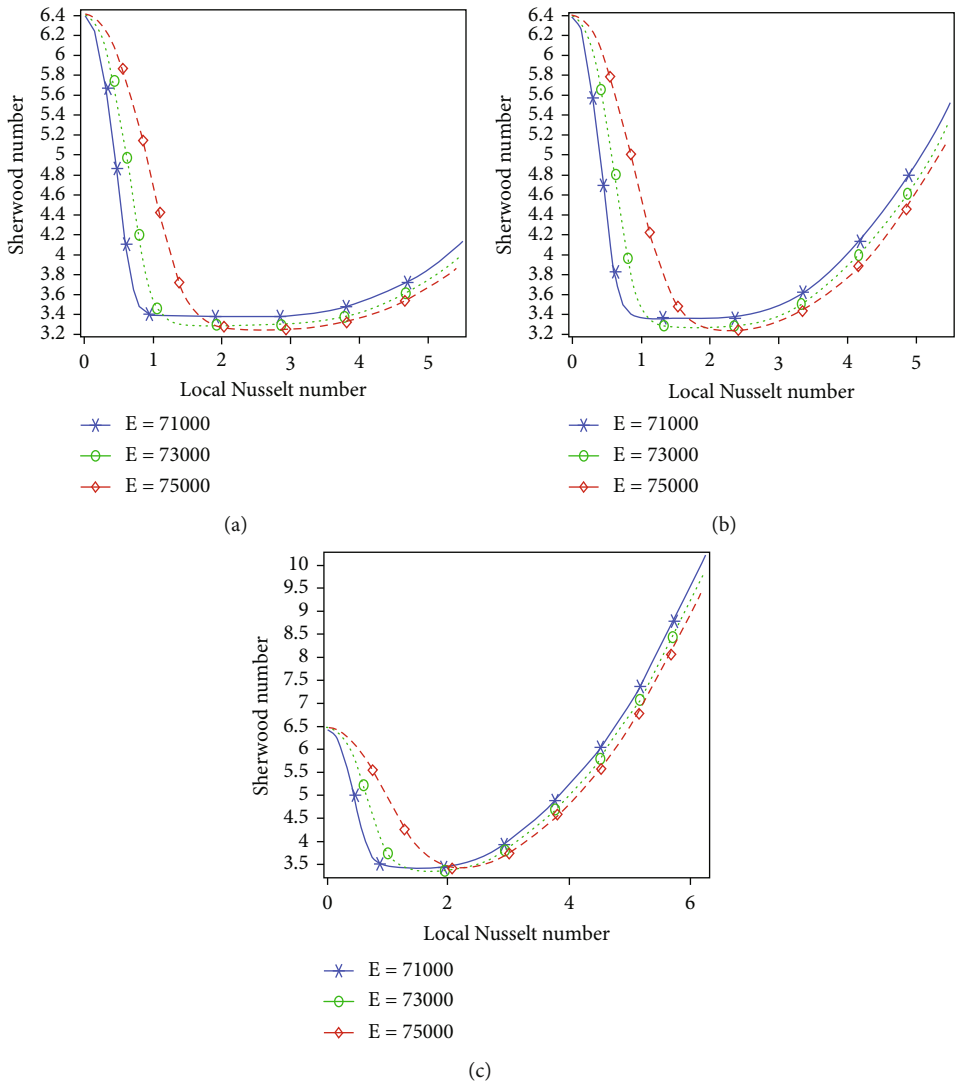

FIGURE 17: Sherwood number vs. the local Nusselt number at upstream along the backward step channel against the axial direction at (a) Re = 100, $I.C = 3\%$, $a = 0.5$; (b) Re = 100, $I.C = 3\%$, $a = 0.6$; and (c) Re = 100, $I.C = 3\%$, $a = 0.7$.

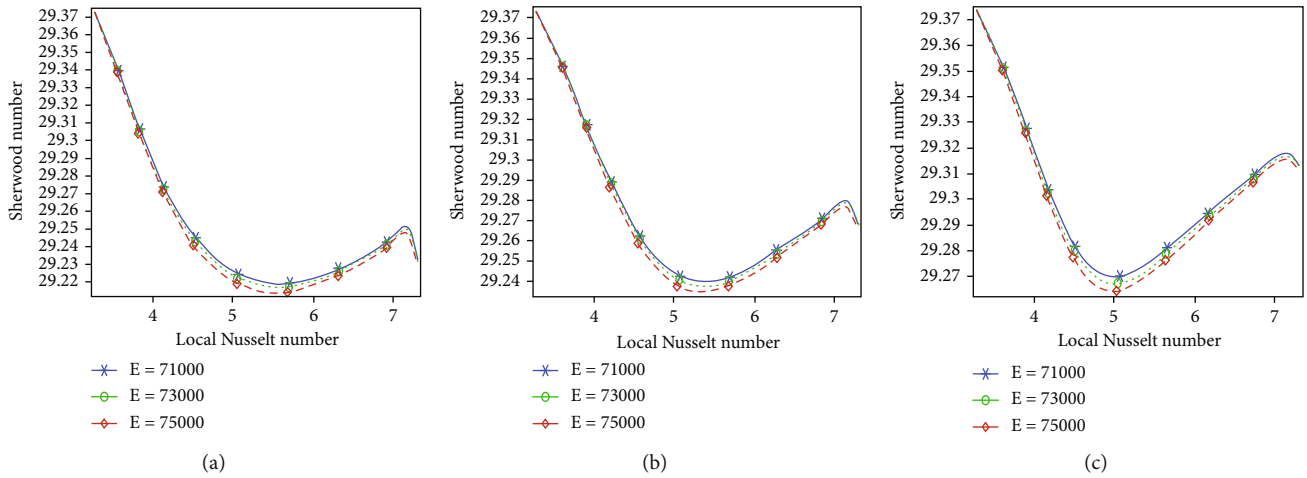

Figure 18: Sherwood number vs. the local Nusselt number at downstream along the backward step channel against the axial direction at (a) Re = 100, $I.C = 1\%$, $a = 0.5$; (b) Re = 100, $I.C = 1\%$, $a = 0.6$; and (c) Re = 100, $I.C = 1\%$, $a = 0.7$.

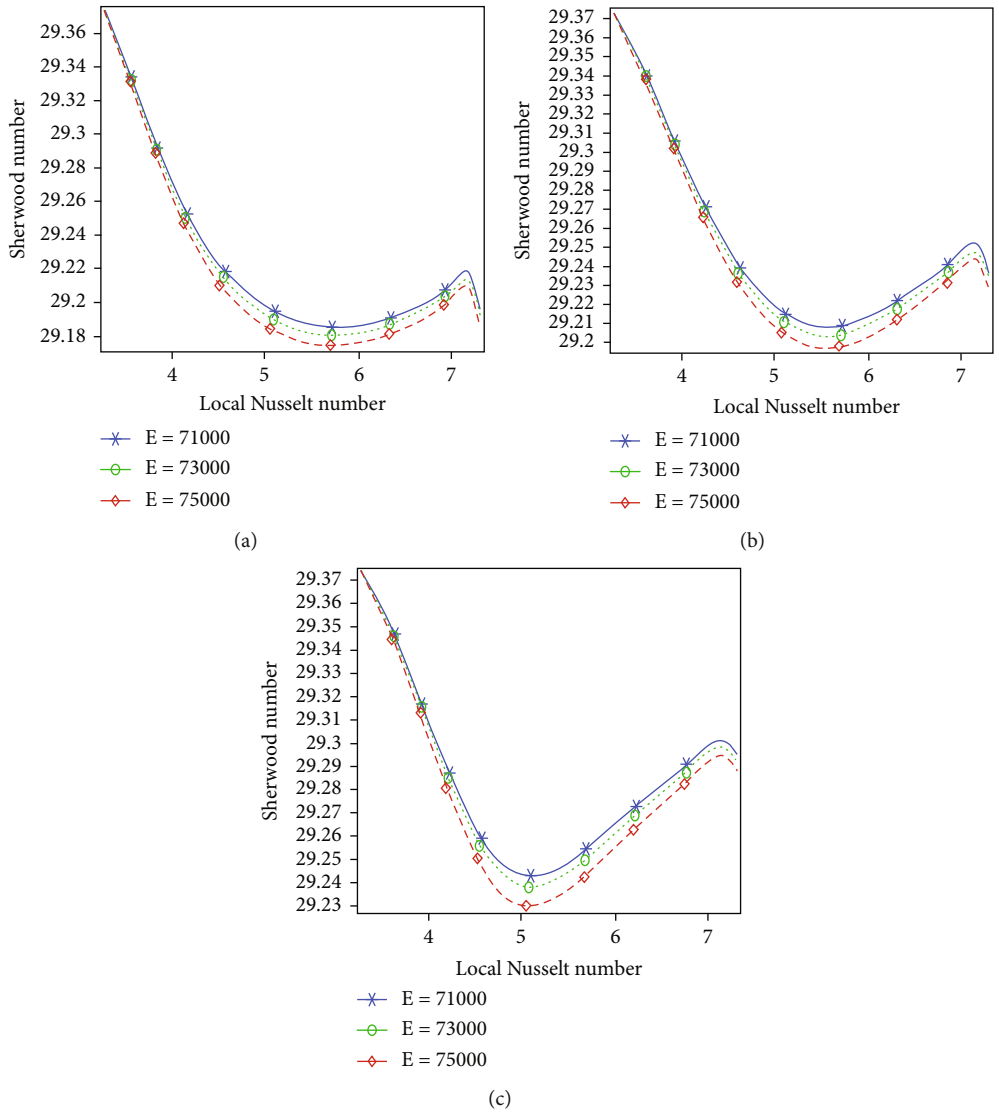

Figure 19: Sherwood number vs. the local Nusselt number at downstream along the backward step channel against the axial direction at (a) Re = 100, $I.C = 3\%$, $a = 0.5$; (b) Re = 100, $I.C = 3\%$, $a = 0.6$; and (c) Re = 100, $I.C = 3\%$, $a = 0.7$.

Table 2: Average Nusselt number at the outlet of the channel.

Re	E	$I.C$	$a = 0.5$ S_h	$a = 0.5$ Nu_z	$a = 0.6$ S_h	$a = 0.6$ Nu_z	$a = 0.7$ S_h	$a = 0.7$ Nu_z
100	71000	1	15.94	6.61	17.88	6.74	21.49	6.96
100	71000	2	14.87	6.52	16.82	6.67	20.57	6.91
100	71000	3	13.93	6.44	15.87	6.60	19.72	6.86
100	73000	1	15.85	6.60	17.79	6.74	21.38	6.95
100	73000	2	14.72	6.51	16.66	6.66	20.38	6.90
100	73000	3	13.75	6.42	15.65	6.58	19.46	6.84
100	75000	1	15.77	6.59	17.69	6.73	21.26	6.95
100	75000	2	14.58	6.50	16.48	6.64	20.15	6.88
100	75000	3	13.56	6.40	15.41	6.56	19.14	6.82
200	71000	1	19.44	9.09	20.78	9.20	23.80	9.42
200	71000	2	17.99	8.95	19.26	9.07	22.07	9.29
200	71000	3	16.78	8.83	18.02	8.95	20.55	9.17
200	73000	1	19.35	9.09	20.68	9.19	23.68	9.41
200	73000	2	17.85	8.94	19.09	9.05	21.85	9.27
200	73000	3	16.61	8.81	17.82	8.93	20.26	9.14
200	75000	1	19.27	9.08	20.59	9.19	23.59	9.41
200	75000	2	17.70	8.93	18.93	9.04	21.67	9.26
200	75000	3	16.41	8.79	17.58	8.91	19.97	9.12
300	71000	1	23.10	11.06	24.73	11.20	26.33	11.32
300	71000	2	21.32	10.89	23.09	11.05	24.55	11.18
300	71000	3	19.85	10.73	21.74	10.92	23.16	11.05
300	73000	1	23.00	11.06	24.61	11.19	26.20	11.32
300	73000	2	21.16	10.88	22.89	11.03	24.32	11.16
300	73000	3	19.65	10.71	21.50	10.89	22.88	11.03
300	75000	1	22.89	11.05	24.48	11.18	26.08	11.31
300	75000	2	20.99	10.86	22.67	11.02	24.09	11.14
300	75000	3	19.43	10.69	21.22	10.87	22.54	11.00
500	71000	1	29.54	14.23	31.97	14.45	33.83	14.61
500	71000	2	27.08	14.00	29.05	14.21	30.91	14.39
500	71000	3	25.04	13.78	26.53	13.98	28.49	14.19
500	73000	1	29.41	14.22	31.84	14.44	33.68	14.60
500	73000	2	26.87	13.98	28.76	14.19	30.56	14.37
500	73000	3	24.76	13.75	26.02	13.94	27.95	14.15
500	75000	1	29.34	14.22	31.87	14.44	33.76	14.61
500	75000	2	26.67	13.96	28.76	14.18	30.52	14.36
500	75000	3	24.54	13.73	26.04	13.93	27.74	14.12

the initial concentration is changing from 1% to 3%. In Figures 21(a) and 21(b), we present the rotation rate in the middle of the downstream by fixing all other parameters with the changing of aspect ratio at Re = 500. It can be seen that the rotation rate at $a = 0.5$ is greater along the length of the channel for all other aspect ratios.

At least we can say a little bit of impact of initial concentration can be seen at the outlet so that the rotation rate is decreased very small. In Figures 22(a) and 22(b), the impact of activation energy on rotation rate is being checked. Figure 22(a) reveals the message that there is no significant impact on rotation rate that can be deducted from increasing activation energy. But for the same when the aspect ratio is increased from 0.5 to 0.7, the movement of rotation rate exists gradually along the length of the channel in Figure 22(b). The rotation rate almost increases rapidly before the outlet of the channel. Finally, we check the impact of initial concentration on rotation rate to fix all other parameters. For this purpose, we have produced Figures 23(a)–23(c). It is clear from the graph that for a particular case of Reynolds number, activation energy, and the aspect ratio, the rotation rate along the length does not show an impact on the rotation rate. However, on observing all the three figures from Figures 23(a)–23(c), the rotation rate

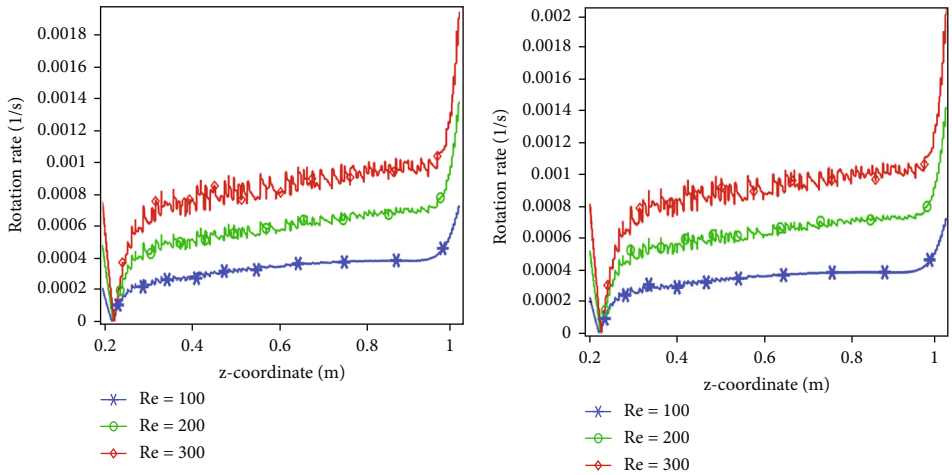

Figure 20: Measurement of rotation rate through the center middle of the downstream of backward step channel at with $a = 0.5$: (a) $I.C = 1\%$ and (b) $I.C = 3\%$.

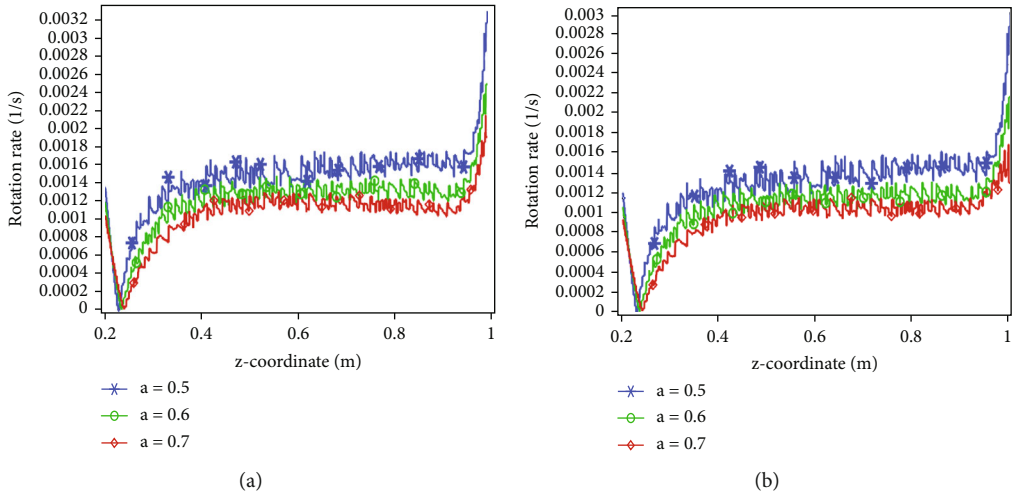

Figure 21: Measurement of rotation rate through the center middle of the downstream of backward step channel for all aspect ratios and Re = 500: (a) $I.C = 1\%$ and (b) $I.C = 3\%$.

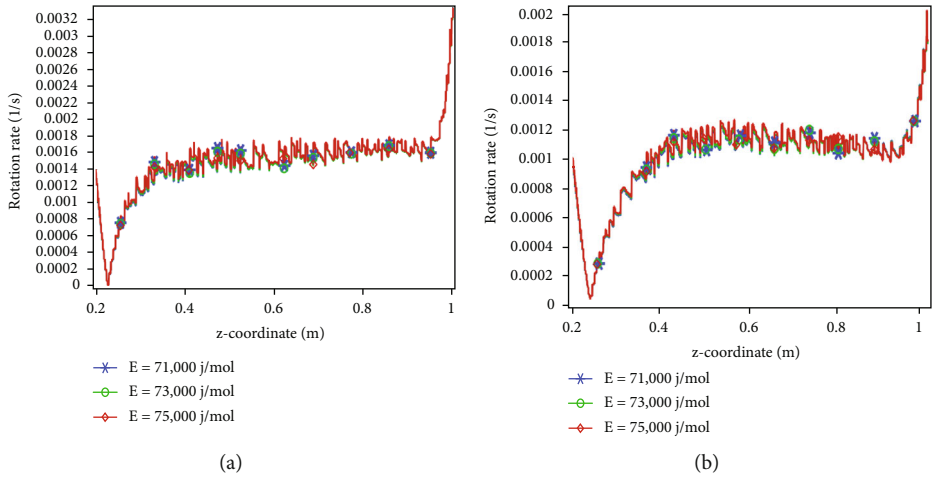

Figure 22: Measurement of rotation rate through the center middle of the downstream backward step channel with different activation energies and Re = 500: (a) $a = 0.5$ and (b) 0.7.

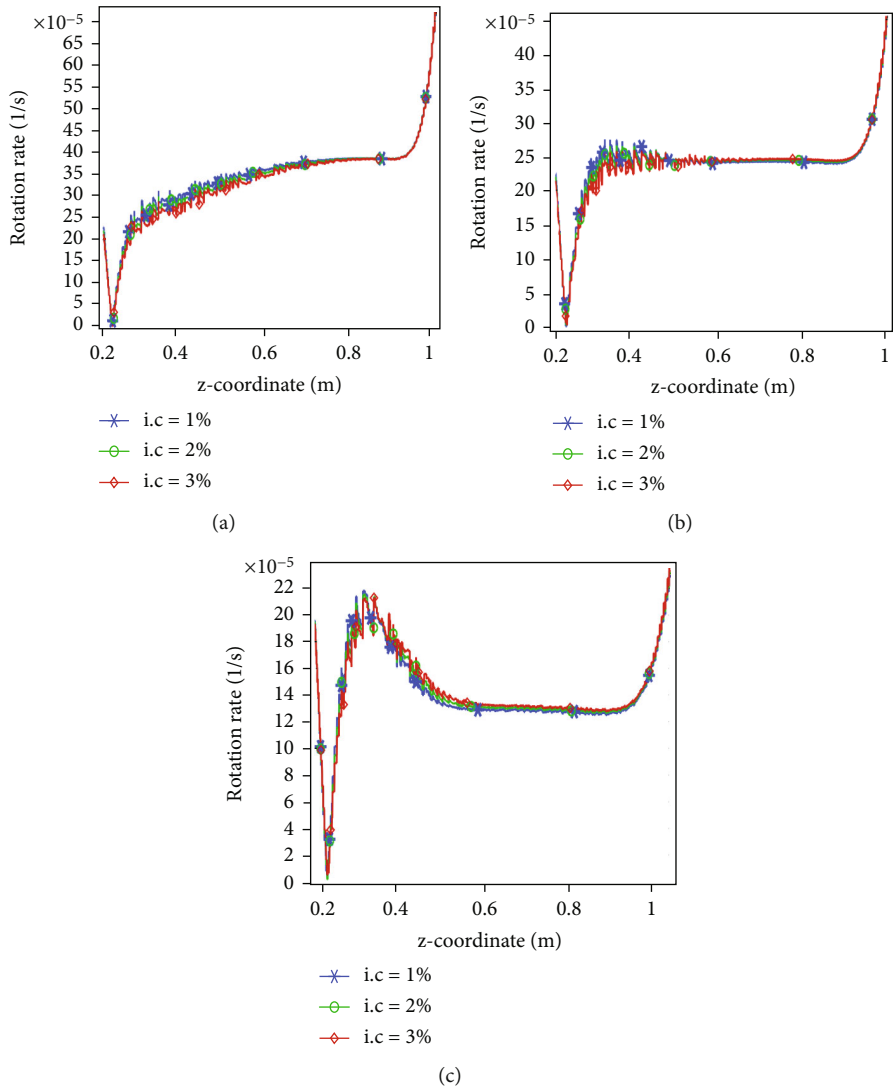

Figure 23: Measurement of rotation rate through the center middle of the downstream of backward step channel for all initial concentration at Re = 100: (a) $a = 0.5$, (b) $a = 0.6$, and (c) $a = 0.7$.

increased and fluctuated especially in the case $a = 0.7$. We concluded that the rotation rate is gradually impacted by the speed of the flow and the aspect ratio of the channel.

4. Conclusions

A chemical reaction of calcium oxide in water was observed in the current simulation to enhance the heat transfer and other properties of the flow of the chemical mixture. For this purpose, a backward step tubular reactor was considered with an aspect ratio of 0.5, 0.6, and 0.7 between the half-width and downstream channel. An inward heat flux boundary condition was applied to the surrounding of this tubular reactor which is capable to provide a cooling environment inside the channel, whereas the mixture of calcium oxide and water is allowed with hot temperature. The constitutive partial differential equations for the mass, momentum, and energy and diffusion equations were used to simulate using the commercial software COMSOL Multiphysics 5.6. The chemical engineering interface was especially used to observe the first-order forward realistic chemical reaction of calcium oxide and water. The forward reaction rate was measured by the Arrhenius equation, and this chemical reaction was enhanced with the use of activation energy in 71,000 J/mol-75,000 J/mol. The initial concentration of the calcium oxide was allowed with 1% to 3% from the entrance of the channel. A nondimensional Reynolds number was kept in 100 to 500 which generates a flow rate of 1.2×10^{-5} to 6.3×10^{-5}. The results were produced for the temperature difference, enthalpy, and Sherwood number vs. the local Nusselt number at the upstream and downstream channel with variation in the selected parameters. Specifically, the rotation rate at the middle of the downstream was also checked against the selected parameters. We can conclude the following points:

(i) It was found the temperature difference at the concentration of hydroxide possesses a linear relationship with the upstream of the backward tubular reactor. The temperature difference upstream of

the channel is increasing with the increase in activation energy and the aspect ratio of the channel. The temperature difference due to the inlet is also improving with the increase in initial concentration

(ii) Because of applying the inward heat flux around the surface of the backward step tubular reactor, a cooling environment was created downstream of the channel and the average temperature was found to be -39 K. There was no direct relationship found between the concentration of calcium hydroxide and temperature difference due to inlet

(iii) A rapid increment in the enthalpy of the reaction was found near the inlet of the channel upstream of the channel. The pattern of distribution of enthalpy is parabolic along the length of the channel. The values of enthalpy at the outlet are positive whereas these are negative downstream of the channel. Enthalpy is increasing either upstream or downstream with the increase in the Reynolds number, aspect ratio, initial concentration, and activation energy

(iv) The Sherwood number against the local number at the upstream or the downstream is increasing with the decreasing the activation energy. The Sherwood number at the outlet of the channel is increasing with an increase in the aspect ratio of the channel. The Sherwood number has greater values downstream when compared with the values upstream

(v) The average Sherwood number and the Nusselt number at the outlet are increasing with the increase in aspect ratio as well as the Reynolds number, while they are decreasing with the increase in initial concentration as well as the initial concentration

(vi) The rotation rate at the middle of the downstream is increasing gradually with the increase in Reynolds number as well as the aspect ratio of the backward step tubular reactor. For all cases, a rapid increment near the outlet of the channel can be seen. The rotation rate almost remains ineffective due to changes in the initial concentration and the activation energy

Data Availability

No data were required to perform this research.

Conflicts of Interest

The authors declare that they have no conflict of interest.

Acknowledgments

This work was supported by Taif University Researchers Supporting Project number (TURSP-2020/247), Taif University, Taif, Saudi Arabia.

References

[1] A. K. Hussein, "Applications of nanotechnology in renewable energies–a comprehensive overview and understanding," *Renewable and Sustainable Energy Reviews*, vol. 42, pp. 460–476, 2015.

[2] M. Kouzu, T. Kasuno, M. Tajika, Y. Sugimoto, S. Yamanaka, and J. Hidaka, "Calcium oxide as a solid base catalyst for transesterification of soybean oil and its application to biodiesel production," *Fuel*, vol. 87, no. 12, pp. 2798–2806, 2008.

[3] Y. Y. Margaretha, H. S. Prastyo, A. Ayucitra, and S. Ismadji, "Calcium oxide from Pomacea sp. shell as a catalyst for biodiesel production," *Engineering*, vol. 3, no. 1, pp. 1–9, 2012.

[4] A. Ouannas, F. Mesdoui, S. Momani, I. Batiha, and G. Grassi, "Synchronization of FitzHugh-Nagumo reaction-diffusion systems via one-dimensional linear control law," *Archives of Control Sciences*, vol. 31, 2021.

[5] M. Angerer, M. Djukow, K. Riedl, S. Gleis, and H. Spliethoff, "Simulation of cogeneration-combined cycle plant flexibilization by thermochemical energy storage," *Journal of Energy Resources Technology*, vol. 140, no. 2, 2018.

[6] M. Schmidt, M. Gollsch, F. Giger, M. Grün, and M. Linder, "Development of a moving bed pilot plant for thermochemical energy storage with CaO/Ca (OH) 2," in *AIP Conference Proceedings*, vol. 1734, p. 050041, Cape Town, South Africa, 2016.

[7] S. Rougé, Y. A. Criado, O. Soriano, and J. Carlos Abanades, "Continuous CaO/Ca(OH)2fluidized bed reactor for energy storage: first experimental results and reactor model validation," *Industrial & Engineering Chemistry Research*, vol. 56, no. 4, pp. 844–852, 2017.

[8] F. Schaube, L. Koch, A. Wörner, and H. Müller-Steinhagen, "A thermodynamic and kinetic study of the de- and rehydration of $Ca(OH)_2$ at high H_2O partial pressures for thermochemical heat storage," *Thermochimica Acta*, vol. 538, pp. 9–20, 2012.

[9] P. Pardo, A. Deydier, Z. Anxionnaz-Minvielle, S. Rougé, M. Cabassud, and P. Cognet, "A review on high temperature thermochemical heat energy storage," *Renewable and Sustainable Energy Reviews*, vol. 32, pp. 591–610, 2014.

[10] A. Odukoya and G. F. Naterer, "Calcium oxide/steam chemical heat pump for upgrading waste heat in thermochemical hydrogen production," *International Journal of Hydrogen Energy*, vol. 40, no. 35, pp. 11392–11398, 2015.

[11] Y. Yuan, Y. Li, and J. Zhao, "Development on thermochemical energy storage based on CaO-based materials: a review," *Sustainability*, vol. 10, no. 8, p. 2660, 2018.

[12] K. Risthaus, I. Bürger, M. Linder, and M. Schmidt, "Numerical analysis of the hydration of calcium oxide in a fixed bed reactor based on lab-scale experiments," *Applied Energy*, vol. 261, p. 114351, 2020.

[13] J. Blamey, M. Zhao, V. Manovic, E. J. Anthony, D. R. Dugwell, and P. S. Fennell, "A shrinking core model for steam hydration of CaO-based sorbents cycled for CO_2 capture," *Chemical Engineering Journal*, vol. 291, pp. 298–305, 2016.

[14] S. A. Salaudeen, B. Acharya, and A. Dutta, "CaO-based CO2 sorbents: a review on screening, enhancement, cyclic stability, regeneration and kinetics modelling," *Journal of CO_2 Utilization*, vol. 23, pp. 179–199, 2018.

[15] C. Chi, Y. Li, X. Ma, and L. Duan, "CO_2 capture performance of CaO modified with by-product of biodiesel at calcium looping conditions," *Chemical Engineering Journal*, vol. 326, pp. 378–388, 2017.

[16] L. Wei, H. Yang, B. Li et al., "Absorption-enhanced steam gasification of biomass for hydrogen production: effect of calcium oxide addition on steam gasification of pyrolytic volatiles," *International Journal of Hydrogen Energy*, vol. 39, no. 28, pp. 15416–15423, 2014.

[17] B. Li, H. Yang, L. Wei, J. Shao, X. Wang, and H. Chen, "Hydrogen production from agricultural biomass wastes gasification in a fluidized bed with calcium oxide enhancing," *International Journal of Hydrogen Energy*, vol. 42, no. 8, pp. 4832–4839, 2017.

[18] Y. A. Criado, M. Alonso, and J. Carlos Abanades, "Kinetics of the CaO/Ca(OH)2hydration/dehydration reaction for thermochemical energy storage applications," *Industrial & Engineering Chemistry Research*, vol. 53, no. 32, pp. 12594–12601, 2014.

[19] F. Schaube, A. Kohzer, J. Schütz, A. Wörner, and H. Müller-Steinhagen, "De- and rehydration of $Ca(OH)_2$ in a reactor with direct heat transfer for thermo-chemical heat storage. Part A: experimental results," *Chemical Engineering Research and Design*, vol. 91, no. 5, pp. 856–864, 2013.

[20] H. Shao, T. Nagel, C. Roßkopf, M. Linder, A. Wörner, and O. Kolditz, "Non-equilibrium thermo-chemical heat storage in porous media: part 2 - A 1D computational model for a calcium hydroxide reaction system," *Energy*, vol. 60, pp. 271–282, 2013.

[21] S. Lin, M. Harada, Y. Suzuki, and H. Hatano, "CaO hydration rate at high temperature (~ 1023 K)," *Energy & Fuels*, vol. 20, no. 3, pp. 903–908, 2006.

[22] H. Matsuda, T. Ishizu, S. K. Lee, and M. Hasatani, "Kinetic study of Ca (OH) _2/CaO reversible thermochemical reaction for thermal energy storage by means of chemical reaction," *Kagaku Kogaku Ronbunshu*, vol. 11, no. 5, pp. 542–548, 1985.

[23] F. Schaube, I. Utz, A. Wörner, and H. Müller-Steinhagen, "De- and rehydration of $Ca(OH)_2$ in a reactor with direct heat transfer for thermo-chemical heat storage. Part B: validation of model," *Chemical Engineering Research and Design*, vol. 91, no. 5, pp. 865–873, 2013.

[24] C. R. Wilke and P. Chang, "Correlation of diffusion coefficients in dilute solutions," *AICHE Journal*, vol. 1, no. 2, pp. 264–270, 1955.

[25] S. W. Churchill and M. Bernstein, "A correlating equation for forced convection from gases and liquids to a circular cylinder in crossflow," *Journal of Heat Transfer*, vol. 99, no. 2, pp. 300–306, 1977.

[26] P. Ramade, P. Patil, M. Shelar, S. Chaudhary, S. Yadav, and S. Trimbake, "Automobile exhaust thermo-electric generator design & performance analysis," *International Journal of Emerging Technology and Advanced Engineering*, vol. 4, no. 5, pp. 682–691, 2014.